




Extracting non-stationary signal under strong noise background: Time-varying system analysis

Zhen Shan¹, Zhongqiu Wang², Jianhua Yang¹ , Dengji Zhou³, and Houguang Liu¹ 

Journal of Vibration and Control
2022, Vol. 0(0) 1–10
© The Author(s) 2022
Article reuse guidelines:
sagepub.com/journals-permissions
DOI: 10.1177/10775463221109715
journals.sagepub.com/home/jvc


Abstract

The extraction of non-stationary feature information under strong noise background is a difficult problem. In this paper, a novel general time-varying scale transformation aperiodic stochastic resonance is proposed to extract and enhance the weak non-stationary signal under strong noise background. The theoretical framework of a parameters time-varying Duffing system is built for aperiodic stochastic resonance. By studying the resonance region migration when scale coefficient takes different values, an optimal scale transformation is achieved. Also, the time-varying system is optimized with cross-correlation coefficient as the index. Compared with the existing methods, the proposed method can be applied to stronger noise background and has stronger noise robustness. When under the same noise background, the proposed method can provide output with higher signal-to-noise ratio and higher cross-correlation coefficient. Finally, experimental analysis of faulty bearing vibration signal verifies the high accuracy, which indicates a good signal extraction and enhancement ability of the proposed method.

Keywords

non-stationary signal, strong noise, vibration signal analysis, feature extraction

1. Introduction

In signal processing, the extraction and enhancement of non-stationary signal under strong noise is an important and difficult problem. Therefore, various signal processing methods have been proposed and applied to the engineering practice. These methods are mainly divided into two types (Lu et al., 2019). One is the method based on digital filter, which can retain signal and attenuate noise (Hu et al., 2018; Lu et al., 2018; Lu and Wang, 2018). Another is signal decomposition method, including empirical mode decomposition (Zhang et al., 2018b, 2020a, 2020b), variational modal decomposition (Gai et al., 2020; Li et al., 2019a), wavelet decomposition (Chen et al., 2019; Liang et al., 2020; Lonare et al., 2021; Qin et al., 2019), and signal sparse decomposition (Fan et al., 2021; Li et al., 2018, 2019c). However, when processing noisy signal with very low signal-to-noise ratio (SNR), the above-mentioned methods fail to provide good results (Cheng et al., 2021; Gong et al., 2019; Wang et al., 2019a; Zhang et al., 2018a). In fact, the extraction and enhancement of non-stationary signal is still a long-term problem to be solved.

Noise, which is usually considered as a negative factor in signal processing, can play a positive role under special

circumstances. For example, when nonlinear system, signal, and noise reach a best match, the noise energy will be transferred to the signal; hence, the SNR increases significantly. This phenomenon is called stochastic resonance (SR) (Li et al., 2019b; Qiao et al., 2019). According to the resonance theory, this phenomenon only occurs when small parameter requirements are met; hence, the signal frequency is lower than 1 Hz and the system parameter has an order of

¹Jiangsu Key Laboratory of Mine Mechanical and Electrical Equipment, School of Mechatronic Engineering, China University of Mining and Technology, Xuzhou, China

²School of Computer Science and Technology, China University of Mining and Technology, Xuzhou, China

³Key Laboratory of Power Machinery and Engineering, Shanghai Jiao Tong University, Shanghai, China

Received: 9 November 2021; revised: 31 March 2022; accepted: 5 June 2022

Corresponding author:

Jianhua Yang, Jiangsu Key Laboratory of Mine Mechanical and Electrical Equipment, School of Mechatronic Engineering, China University of Mining and Technology, No.1 Daxue Road, Xuzhou 221116, China.
Email: jianhuayang@cumt.edu.cn

magnitude of 1. However, the signals in engineering practice that can reflect the fault characteristics of rotating machinery is mostly in the range of tens to hundreds of Hertz. Also, it often has non-stationary characteristics, including frequency and amplitude modulation.

To break through the limitation that SR can only process low-frequency signals, a series of scale transformation are proposed. Leng et al. proposed twice sampling technology (Leng et al., 2004; Wang and Leng, 2003). Lu et al. proposed the normalized variable scale technology (Lu et al., 2014). Huang et al. proposed the general scale transformation. Compared to the normalized scale transformation stochastic resonance, the general scale transformation stochastic resonance can obtain a better output with higher *SNR*, and it has been applied in bearing fault diagnosis (Yang et al., 2020a). However, the parameters in the above methods are fixed, which determines that it is more suitable for stationary signals processing, such as vibration signal of rotating machinery with fixed speed. However, because of unstable loads and other factors, rotation speed often changes in real time, causing characteristic frequency of rotating parts changes in real time (Li et al., 2019d; Wang et al., 2019b; Yu, 2019).

To realize the aperiodic stochastic resonance (ASR), researchers have done a lot of research. Yang et al. successfully realized the SR of the variable frequency signal by using the piecewise scale transformation (Yang et al., 2020b). In that paper, original signal was cut into several sub-segments and each sub-segment was regarded as stationary. Subsequently, by optimizing the parameters of each sub-segment, sub-output of piecewise scale transformation SR for each sub-segment was obtained. At last, all sub-outputs were spliced into the final output. Similar segmentation processing methods appeared in vibration resonance (Jia et al., 2019). However, such methods have great human factors when dividing signal. More extremely, Zhang et al. cut each data point into separate sub-segment, and proposed a new varying parameters and normalization stochastic resonance (VPNSR), which was based on the normalized transformation (Zhang et al., 2016). This method maps the time-varying frequency to a constant low frequency with the help of time-varying parameters, and successfully realizes the ASR of linear frequency modulation (LFM) signal. However, in this work, the noise intensity is weak, and the signal frequency modulation mode is linear. So, faced with nonlinear frequency modulation signal and strong noise background, whether the method is effective remains further discussion.

In fact, most of the methods mentioned above are designed for stationary signals processing, but not for non-stationary signals processing. Under non-stationary conditions, such as rotating machinery, the time-varying speed causes the instantaneous characteristic frequencies of various components to have time-varying characteristics. Also, strong noise and low *SNR* exist in non-stationary conditions. These negative factors bring great challenges to

signal processing, and cause signal processing methods based on fixed parameter not to work in non-stationary signal processing.

To solve the above problems, a new general time-varying scale transformation aperiodic stochastic resonance (GTVST-ASR) is proposed. Firstly, in Duffing system, a new general time-varying scale transformation (GTVST) is needed. Then, parameter optimization should be carried out to obtain the optimal ASR. Also, comparison between the proposed method and existing methods is of great importance. To verify the effectiveness of the GTVST-ASR, faulty bearing signals under strong noise and complex variable speed condition should be processed with GTVST-ASR. The innovations of this paper are summarized as follows:

- A novel time-varying parameter nonlinear system is built, and aperiodic stochastic resonance can occur in it under strong noise background.
- Compared with the previous aperiodic resonance methods, this proposed method provides higher quality output with higher *SNR*, higher cross-correlation coefficient (*C*). Also, the proposed method can be applied to stronger noise background and has stronger noise robustness.
- The proposed method can process more complex non-stationary signal, it is superior to the previous stochastic resonance in scope of application.

The structure of this paper is arranged as follows. In Section 2, the theoretical framework of GTVST-ASR is established, including derivation and dynamic analysis. In Section 3, the migration process of resonance region under different parameters is studied, based on which, the parameters are optimized. In Section 4, the experimental validation is carried out, where GTVST-ASR is employed to process the faulty bearing signal under the condition of variable speed and strong noise, and hence further verify the practical value. Finally, the discussion and conclusions are provided in Section 5 and Section 6, respectively.

2. Methodology of general time-varying scale transformation aperiodic stochastic resonance

The time-varying parameter bistable system excited by noise and variable frequency signal can be expressed by equation (1)

$$\begin{aligned} \frac{dx}{dt} &= a(t)x - b(t)x^3 + u(t) + n(t) \\ &= a(t)x - b(t)x^3 + A \cos\left(\int_0^t 2\pi f(t)dt\right) + \sqrt{2D}\xi(t) \end{aligned} \quad (1)$$

Here, $a(t)$ and $b(t)$ are large parameters that change with time, the time-varying instantaneous frequency $f(t)$ is greater than 1. A is signal amplitude of the pure signal $u(t)$,

$\zeta(t)$ is the standard Gaussian white noise with zero mean, where $\langle \zeta(t) \rangle = 0$, $\langle \zeta(t), \zeta(0) \rangle = \delta(t)$. D is the noise intensity, and $\delta(t)$ represents the Dirac equation.

Considering the small parameter requirements of the resonance theory, classical SR excited by fixed frequency signal and noise in Duffing system can be expressed as equation (2)

$$\begin{aligned} \frac{dx}{dt} &= a_1x - b_1x^3 + u(t) + n(t) \\ &= a_1x(t) - b_1x^3(t) + A \cos(2\pi f_1 t) + \sqrt{2D}\zeta(t) \end{aligned} \quad (2)$$

Here, the order of magnitude of fixed system parameters a_1 and b_1 is 1, and the magnitude of the constant signal frequency f_1 is less than 1. This is the small parameter requirement in resonance theory. As is shown in equation (2), stochastic resonance that occurs in bistable system meets the small parameters requirement. Where the system parameters a_1 and b_1 is in order of 1, and the signal frequency f_1 is far less than 1 Hz, and the signal amplitude A is much less than 1. However, equation (1) has large parameters, hence does not meet the small parameters requirements. So, equation (1) cannot directly realize resonance. To make equation (1) meet the small parameters requirements and realize aperiodic resonance, GTVST is proposed in this paper.

Firstly, variable substitution is introduced in equation (3)

$$\begin{aligned} x(t) &= z(\tau), m(t) = m_0 f(t), \tau = m(t)t, \\ a(t) &= a_1 m(t), b(t) = b_1 m(t) \end{aligned} \quad (3)$$

Here, t and τ denote different time scales, $x(t)$ and $z(\tau)$ represent signal s in different time scales, $a(t)$ and $b(t)$ stand for the parameters in time-varying Duffing system. The scale coefficient m_0 is a fixed positive value, the time-varying instantaneous frequency $f(t)$ is greater than 1, so $m(t)$ is always greater than 0.

Then, substitute equation (3) into equation (1), hence equation (4) is

$$\begin{aligned} \frac{dz(\tau)}{d\tau} &= \frac{a(\tau)}{m(\tau)}z(\tau) - \frac{b(\tau)}{m(\tau)}z^3(\tau) \\ &+ \frac{A}{m(\tau)} \cos\left(\int_0^\tau 2\pi \frac{f(\tau)}{m(\tau)} \tau\right) + \sqrt{\frac{2D}{m(\tau)}}\zeta(\tau) \end{aligned} \quad (4)$$

In equation (4), $\frac{a(\tau)}{m(\tau)}$, $\frac{b(\tau)}{m(\tau)}$, and $\frac{f(\tau)}{m(\tau)}$ are small fixed parameters, which correspond to a_1 , b_1 , and f_1 in equation (2), respectively. However, the signal amplitude $\frac{A}{m(\tau)}$ and noise intensity $\frac{D}{m(\tau)}$ in equation (4) are time-varying, but constant in equation (2). Therefore, the dynamic characteristics of equation (4) and equation (2) are different. To remove the time-varying project $\frac{1}{m(\tau)}$ and $\sqrt{\frac{1}{m(\tau)}}$ in equation (4), amplify the signal and noise by $m(\tau)$ and $\sqrt{m(\tau)}$ times, respectively; hence, equation (5) is obtained

$$\begin{aligned} \frac{dz(\tau)}{d\tau} &= \frac{a(\tau)}{m(\tau)}z(\tau) - \frac{b(\tau)}{m(\tau)}z^3(\tau) \\ &+ A \cos\left(\int_0^\tau 2\pi \frac{f(\tau)}{m(\tau)} \tau\right) + \sqrt{2D}\zeta(\tau) \\ &= a_1z(\tau) - b_1z^3(\tau) + A \cos\left(\int_0^\tau 2\pi \frac{1}{m_0} \tau\right) + \sqrt{2D}\zeta(\tau) \end{aligned} \quad (5)$$

Comparison shows that $\frac{a(\tau)}{m(\tau)} = a_1$, $\frac{b(\tau)}{m(\tau)} = b_1$, and $\frac{f(\tau)}{m(\tau)} = \frac{1}{m_0}$ in equation (5) are fixed parameters with small values, which are the same as that in equation (2). Therefore, equation (5) and equation (2) have the same dynamic characteristics. Also, equation (5) is transformed from equation (1). So, equation (1) can be equivalent to equation (2) with GTVST.

The above derivation mainly includes two parts. One is the time scale transformation for equation (1), where the time scale is switched from t to τ . The second is the amplitude transformation in scale τ . In fact, the above two parts can be finished in one part, that is the amplitude transformation in scale t , and get equation (6)

$$\begin{aligned} \frac{dx}{dt} &= a(t)x - b(t)x^3 + m(t)A \cos\left(\int_0^t 2\pi f(t)t\right) \\ &+ \sqrt{2Dm(t)}\zeta(t) \end{aligned} \quad (6)$$

Here, $a(t)$, $b(t)$, and $f(t)$ are time-varying large parameters.

In this section, based on GTVST, the dynamic characteristics of Langevin equation of large parameter variable frequency signal are deduced. The deduction shows that the time-varying system excited by aperiodic signal has the same dynamics characteristics as the classical Duffing system, which proves the realization possibility of GTVST-ASR.

3. Optimal general time-varying scale transformation aperiodic stochastic resonance

3.1. Framework of optimization in general time-varying scale transformation aperiodic stochastic resonance

In ASR, parameter optimization often plays an important role when massive parameters are to be determined. Here, some commonly used optimization algorithms include genetic algorithm and quantum swarm algorithms. However, parameter optimization based on above algorithms may fall into local optimum (Cao et al., 2018; Chen et al., 2018). Also, these methods are based on single thread and much computing power are wasted. To solve it, based on global parameter search method and parallel computing, this section introduces the optimal GTVST-ASR.

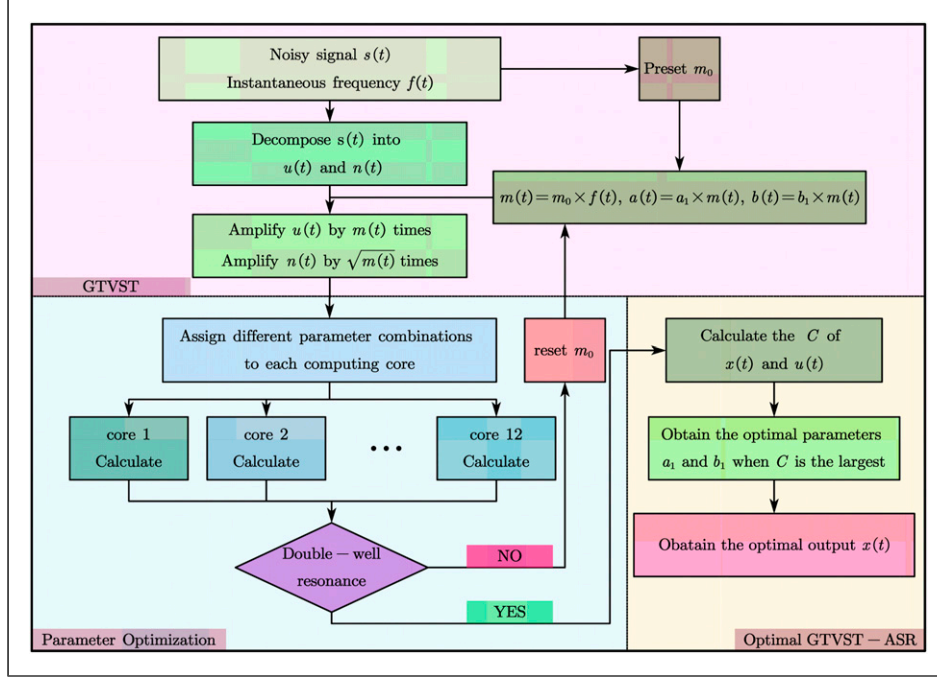


Figure 1. Flow chart of General time-varying scale transformation aperiodic stochastic resonance.

Figure 1 illustrates the flow chart of GTVST-ASR, which includes three parts, namely, GTVST, parameters optimization, and the optimal GTVST-ASR.

Step 1. General time-varying scale transformation.

According to the frequency range of signal, decompose the original signal $s(t)$ into filtered pure signal $u(t)$ and noise $n(t)$ by band-pass filter. Then, amplify $u(t)$ and $n(t)$ by $m(\tau)$ and $\sqrt{m(\tau)}$ times, respectively.

Step 2.1. **Optimization of m_0 .** Based on different m_0 , calculate the GTVST-ASR output with different a_1 and b_1 in all cores, and obtain the cross-correlation coefficient (C) between the output $x(t)$ and pure signal $u_0(t)$. Choose the m_0 as the optimal parameters when double well resonance area becomes the main part. The C is defined as follows

$$C = \frac{\sum_{i=1}^N (u_0(i) - \bar{u}_0)(x(i) - \bar{x})}{\sqrt{\sum_{i=1}^N (u_0(i) - \bar{u}_0)^2 (x(i) - \bar{x})^2}} \quad (7)$$

Here, $u_0(i)$ and $x(i)$ represent the pure signal and the resonance output, respectively, \bar{u}_0 and \bar{x} represent their mean value.

Step 2.2. **Optimization of a_1 and b_1 .** Based on the optimal m_0 and all combinations of a_1 and b_1 , obtain the outputs and C , choose the a_1 and b_1 as the optimal when C reaches the peak in double well resonance region.

Step 3. Obtain the optimal GTVST-ASR output.

Based on the optimal m_0 , a_1 , and b_1 , obtain the optimal GTVST-ASR output.

3.2. Parameter optimization

3.2.1. **General time-varying scale transformation of simulation signal.** Firstly, the pure signal $u_0(t)$ is defined as follows

$$u_0(t) = A \cos\left(\int_0^t 2\pi f(t) dt\right) \quad (8)$$

Here, A and $f(t)$ represent the amplitude and instantaneous frequency, respectively. The amplitude A is 0.5, the sampling frequency f_s is 10,000 Hz, the signal length N is 20,000, and $f(t)$ is defined in equation (9)

$$f(t) = 20t + 50 \quad (9)$$

To simulate a strong noise background, add white Gaussian noise into $u_0(t)$ and obtain a noisy signal $s(t)$ with SNR of -25 dB.

According to $f(t)$, decompose the noisy signal $s(t)$ into filtered pure signal $u(t)$ and noise $n(t)$ with band-pass filter, the filter center frequency of which is equal to $f(t)$. Figure 2(a) and Figure 2(b) show the time domain waveform of $s(t)$ and $u(t)$, respectively, Figure 2(c) and Figure 2(d) show their time-frequency diagram, respectively. Obviously, Figure 2(a) contains so much noise that no clear time-frequency characteristics can be found in Figure 2(c). After decomposed, obvious amplitude modulation exists in the $u(t)$ in Figure 2(b), and time-frequency curve shown in Figure 2(d) is unstable.

3.2.2. **Optimization of m_0 .** To realize double well resonance and avoid signal well resonance, m_0 should be optimized

firstly. The indicators used here is C , which has been defined in equation (7).

Figure 3 shows the migration of resonance region when m_0 takes 5, 20, 50, and 100. In Figure 3(a), $m_0 = 5$, the verification shows that resonance occurs in single potential well when C reaches the peak. In Figures 3(b) and (a) similar result occurs when $m_0 = 20$, but one thing different is that another resonance region appears when $a_1 \rightarrow 0^+$, which

is proved to be double well resonance region. In Figure 3(c), $m_0 = 50$, the single potential well resonance region migrates in the negative direction of the b_1 -axis, and double potential well resonance region takes more region of $0 < a_1 < 1$ and $b_1 > 2$. In Figure 3(d), $m_0 = 100$, single potential well resonance region shrinks to the finite region of $0.5 < a_1 < 1.5$, $b_1 < 2$, but double potential well resonance region takes up most of the region of $0 < a_1 < 1$, $b_1 > 2$, and it can ensure $C > 0.9$.

To limit the divergence within a finite parameter region, take 100 as the optimal m_0 .

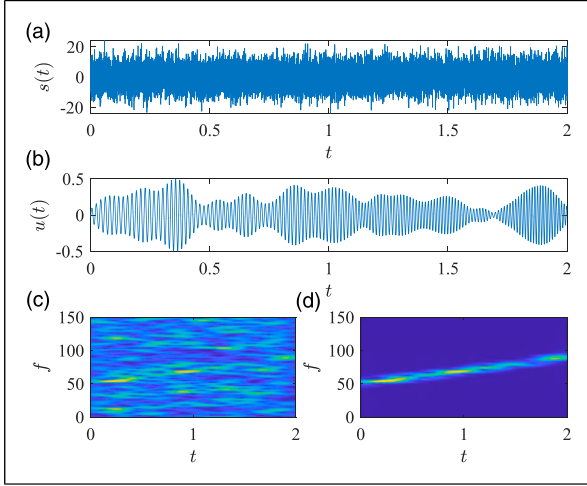


Figure 2. (a) Time domain diagram of noisy signal $s(t)$, $SNR = -25$ dB. (b) Time domain diagram of filtered signal $u(t)$. (c) Time-frequency diagram of noisy signal $s(t)$. (d) Time-frequency diagram of filtered signal $u(t)$.

3.2.3. Optimization of a_1 and b_1 . In ahead section, m_0 has been optimized and set to 100, when the double well resonance region mainly exists in $0 < a_1 < 1$, $2 < b_1 < 10$. Within this region, take 0.01 and 0.1 as the step of a_1 and b_1 , respectively.

Figure 4 shows the surf plot of C in the a_1 - b_1 plane and its projection at $C = -0.5$. Resonance region distribution of system parameters a_1 and b_1 presents two peaks, namely, double well resonance region and signal well resonance region. Previous section has shown the shortcomings of signal well resonance. So, parameters in double well resonance region are more recommended. In double well resonance region, the contour of $C = 0.9$ divides a parameter area, C reaches the maximum of 0.92,511 when $a_1 = 0.1$, $b_1 = 6.3$.

Based on the optimal parameters that $a_1 = 0.1$, $b_1 = 6.3$, $m_0 = 100$, GTVST-ASR of $s(t)$ occurs, and the output $x(t)$ is drawn in Figure 5. Compared to Figure 2(b), the waveform

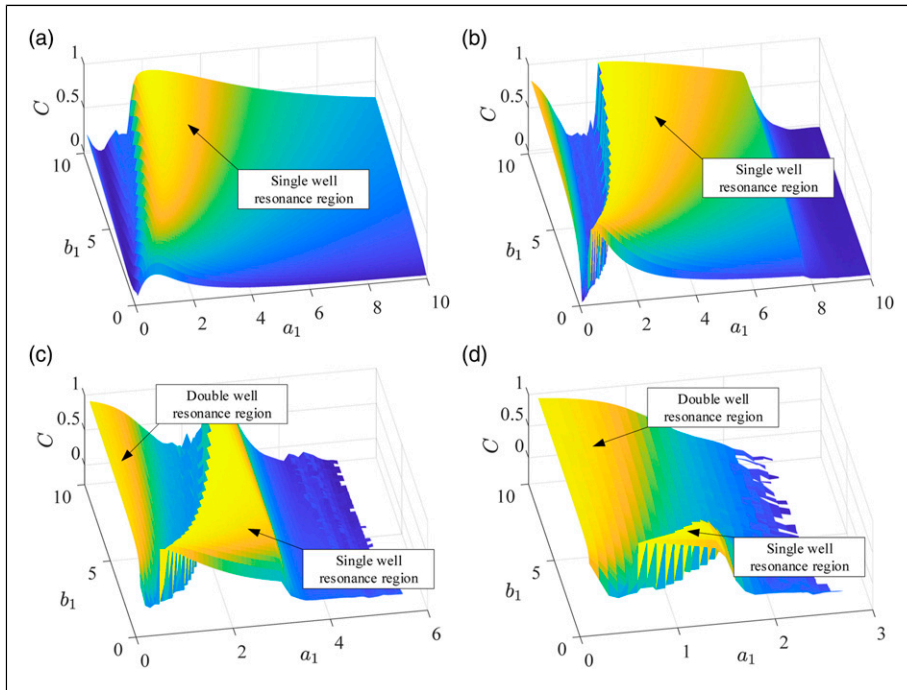


Figure 3. Migration of resonance region with different m_0 . Simulation parameters are (a) $m_0 = 5$, (b) $m_0 = 20$, (c) $m_0 = 50$, (d) $m_0 = 100$.

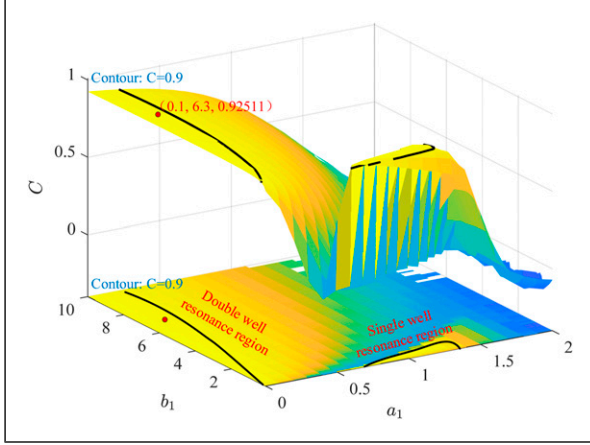


Figure 4. Surf plot of C in the a_1 - b_1 plane. The simulation parameter is $m_0 = 100$.

amplitude in Figure 5(a) is more stable. Also, the characteristic curve in Figure 5(b) is more centralized and continuous than that of Figure 2(c) and Figure 2(d). Therefore, a conclusion is drawn that GTVST-ASR can enhance the time-frequency characteristics of non-stationary signal under strong noise.

3.3. Comparison of aperiodic resonance methods

The above chapters introduce the theoretical framework and implementation method of optimal GTVST-ASR, and the advantages of this method need to be proved. In this section, the proposed method is used, and classical SR and VPNSR are selected as comparison methods to process the frequency conversion signal under strong noise background. The indexes SNR_{input} and the SNR_{output} are defined in equation (10)

$$\left\{ \begin{array}{l} SNR_{input} = 10 \log_{10} \frac{\sum_{i=1}^N u_0^2(i)}{\sum_{i=1}^N (s(i) - u_0(i))^2} \\ SNR_{output} = 10 \log_{10} \frac{\sum_{i=1}^N x^2(i)}{\sum_{i=1}^N (s(i) - x(i))^2} \end{array} \right. \quad (10)$$

where u_0 , s , x are pure signal, noisy signal, and resonance output, respectively.

The signal processed in this section is linear frequency modulation signal, which is defined in equation (8) and equation (9). The system parameter a_1 of GTVST-ASR and classical SR is set to 0.1, and $a = b = b_1 f(t)$ in VPNSR. Here, $0.1 \leq b_1 \leq 10$, step size is 0.1.

Figure 6 (a) and (b) show the curves of C and SNR_{output} versus the parameter b_1 when the $SNR_{input} = -10$ dB. It

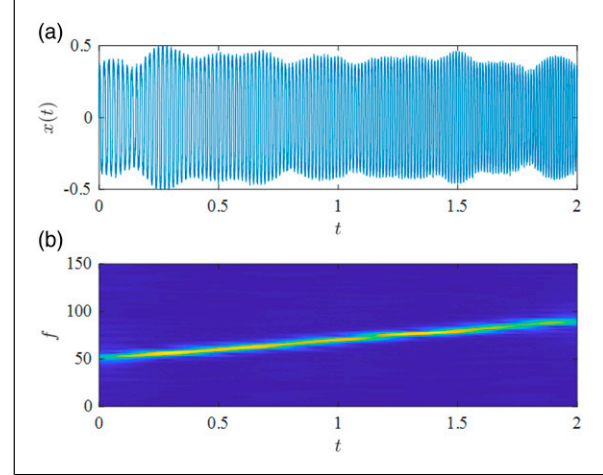


Figure 5. General time-varying scale transformation aperiodic stochastic resonance under strong noise background. (a) Time domain waveform of $x(t)$. (b) Time-frequency diagram of $x(t)$. Simulation parameters are $m_0 = 100$, $a_1 = 0.1$, $b_1 = 6.3$.

shows that the proposed method can obtain the maximal value $C = 0.93$ and $\max SNR_{output} = 8$ dB, which are always greater than that of classical SR and VPNSR. Figure 6(c) shows the maximal value C when SNR_{input} takes different values in $[-25$ dB, 0 dB]. In Figure 6(c), GTVST-ASR can always obtain a well output with $C > 0.9$. However, the classical SR and VPNSR are greatly affected by noise and the output quality is unstable.

4. Experimental verification

Fault bearing vibration signal mainly includes bearing natural vibration signal, fault characteristic signal, and environmental noise. Based on stochastic resonance, fault diagnosis of bearing under stable working condition has been realized, but the fault diagnosis of bearing at variable speed is still difficult. To verify the value of the GTVST-ASR in engineering application, faulty bearing vibration signal is processed, which is collected from bearing testbed of China University of Mining and Technology.

Figure 7 shows the testbed, it includes driving and loading parts, bearing experiment module, signal measurement, acquisition system, etc. The driving motors model are 198BGL-H5P515/120 and the rated power is 5.5 kW. The models of signal acquisition card and acceleration sensor are NI-9234 and DH-1A206 E, respectively. As shown in Figure 7(c), on the outer ring of N306 E faulty bearing, the scratch fault is artificially machined, the circumferential width, axial width, and radial depth of which is 1.2 mm, 19 mm, and 0.5 mm, respectively.

Types of speed change include linear acceleration and nonlinear speed modulation. Its instantaneous rotation frequency f_{r1} and f_{r2} follow equation (10) and equation (11), respectively.

$$f_{r1} = 4.7t + 14.4 \quad t \in [0, 2]$$

$$f_{r2} = \begin{cases} 4.7t + 14.4 & t \in [0, 1.5] \\ 30 & t \in [1.5, 2] \end{cases} \quad (11)$$

frequency f_c to the rotation frequency f_r , which is defined in equation (12) (Huang et al., 2018; Yang et al., 2018)

$$order = \frac{f_c}{f_r} = \frac{z}{2} \left(1 - \frac{d}{D_m} \cos \alpha \right) \quad (12)$$

To extract the fault characteristic frequency f_c , fault order is necessary. Fault order is the ratio of the fault characteristic

Here, structural parameters z , d , D_m , and α stand for number of rolling elements, rolling element diameter,

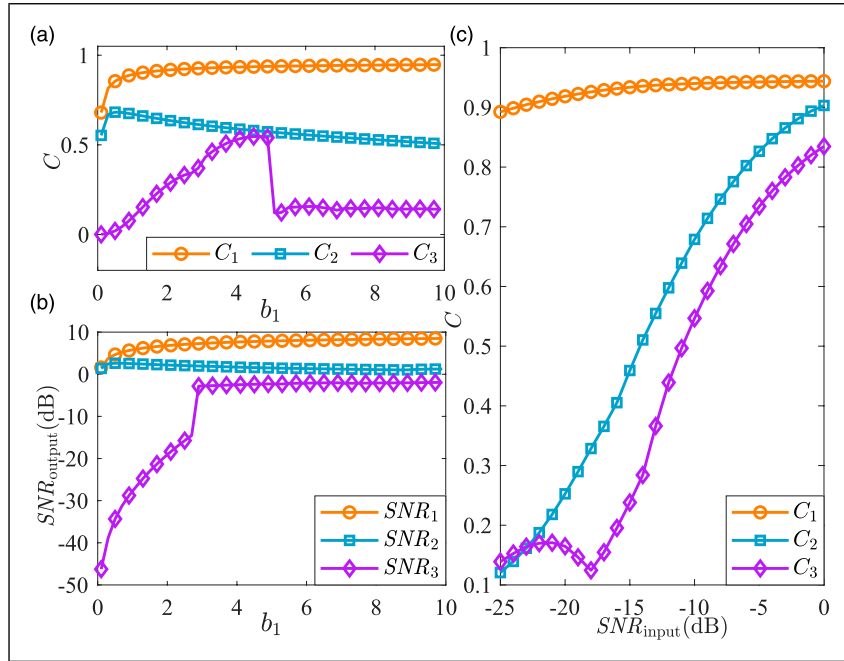


Figure 6. Output results of different ASR systems. In (a) and (b), $SNR = -10$ dB, $\sigma_1 = 0.1$, $b_1 \in [0.1, 10]$. In (c), $SNR \in [-25$ dB, 0 dB], $\sigma_1 = 0.1$. Here, C_1 , C_2 , C_3 , SNR_1 , SNR_2 , and SNR_3 are cross-correlation coefficient and signal-to-noise ratio of the proposed general time-varying scale transformation aperiodic stochastic resonance, varying parameters and normalization stochastic resonance, and classical stochastic resonance, respectively.

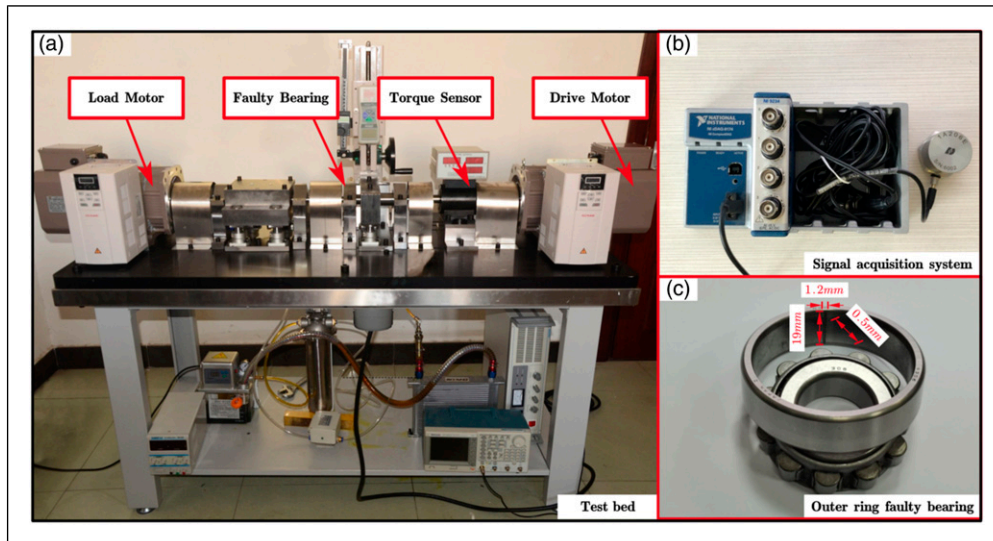


Figure 7. Bearing test bench.

Table 1. Structural parameters of faulty bearing N306 E.

Model	D_0 (mm)	D_i (mm)	D_m (mm)	d (mm)	α	z
N306 E	72	30	52	10	0°	11

bearing raceway pitch diameter, and contact angle, respectively. These parameters of N306 E are listed in Table 1.

After calculation, the order of outer ring fault equals 4.44, substitute it into equation (7), the characteristic frequency f_c of outer ring fault can be obtained in equation (13) and equation (14).

$$f_{c1} = 20.9t + 64 \quad t \in [0, 2] \quad (13)$$

$$f_{c2} = \begin{cases} 22.2t + 100 & t \in [0, 1.5] \\ 133.3 & t \in [1.5, 2] \end{cases} \quad (14)$$

Figure 8 shows the GTVST-ASR outputs of faulty bearing signal under linear acceleration working conditions. In Figure 8(a), bearing signal contains strong noise and there is no obvious regular impact. In Figure 8(c), the time-frequency information of bearing fault is completely submerged by strong noise. After processed by GTVST-ASR, the output shows obvious and regular time domain waveform in Figure 8(b). Also, Figure 8(d) shows a clear curve in time-frequency diagram, and the time-frequency characteristics of this curve is exactly corresponded to the f_{c1} of outer ring fault.

Figure 9 shows the GTVST-ASR outputs of faulty bearing signal under nonlinear speed modulation working condition. Although the working condition is different from that in Figure 8, the conclusions are similar. GTVST-ASR also shows excellent results in processing signals under complex working condition.

5. Discussions

In GTVST-ASR, instantaneous frequency of the target signal is necessary. It means that the instantaneous rotational speed is required when GTVST-ASR is applied to signal analysis of rotating machinery. But in some cases, this requirement cannot be met because not every machine has a speed measuring device. Fortunately, the measurement of mechanical instantaneous rotation frequency is not difficult, which is a very mature technology. Also, for many large machines, instantaneous rotation frequency measuring device is a common configuration. Therefore, the above requirements are reasonable and achievable, and it will not limit the application and promotion of GTVST-ASR.

In GTVST-ASR, the signal and noise are separated and multiplied by different multiples. It is undeniable that this operation will directly improve the SNR, weaken the strong noise. However, the above operations are completely based

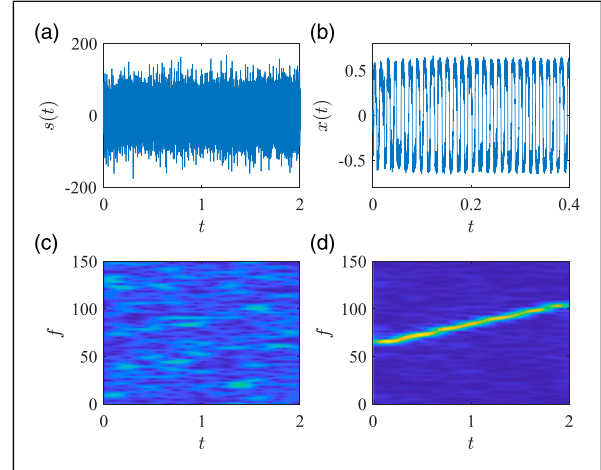


Figure 8. Bearing fault diagnosis with general time-varying scale transformation aperiodic stochastic resonance under linear acceleration working conditions.

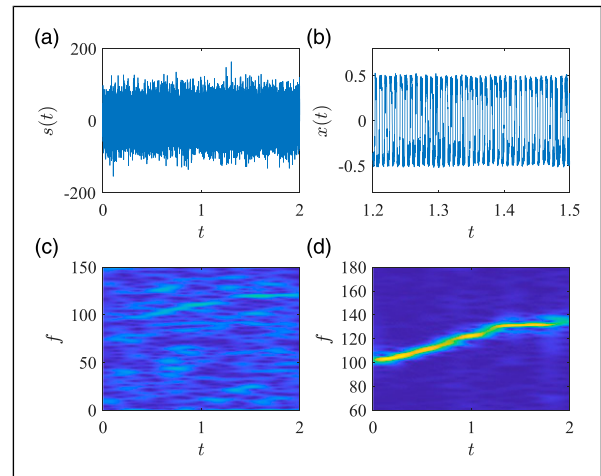


Figure 9. Bearing fault diagnosis with general time-varying scale transformation aperiodic stochastic resonance under nonlinear speed modulation working condition.

on the derivation, not opportunism. The results also show that this method can significantly enhance the signal and obtain a output with more clearer fault characteristics.

6. Conclusions

In this paper, GTVST-ASR is proposed to extract and enhance aperiodic signals under strong noise. Compared with our previous research work on ASR, some theoretical innovation and interesting improvement are obtained.

Theoretical derivation shows this proposed GTVST can realize ASR in parameter time-varying nonlinear system, its dynamic characteristics are similar to those of traditional

SR. Then, the numerical analysis results show that GTVST-ASR can enhance noisy variable frequency signal.

Comparison with the existing ASR methods shows that the proposed method can provide higher quality output with higher SNR and C under the same noise background. At the same time, the proposed method can be applied to stronger noise background and has higher noise robustness. Although the strong noise covers the signal in the spectrum and time-frequency diagram, the proposed method can still accurately recover the signal, but other existing ASR methods cannot achieve the same effect.

In addition, experimental verification shows that this method can be applied to rotating machinery signal processing under complex variable speed conditions. The time domain and time-frequency domain features of bearing fault signal can be extracted and obviously enhanced.

ORCID iDs

Jianhua Yang  <https://orcid.org/0000-0001-5389-9142>

Houguang Liu  <https://orcid.org/0000-0002-5450-5958>

Acknowledgments

We acknowledge financial support by the National Natural Science Foundation of China (Grant No. 12072362), the Priority Academic Program Development of Jiangsu Higher Education Institutions.

Declaration of conflicting interests

The author(s) received no financial support for the research, authorship, and/or publication of this article.

Funding

The author(s) disclosed receipt of the following financial support for the research, authorship, and/or publication of this article: This work was supported by the National Natural Science Foundation of China (Grant No. 12072362), the Priority Academic Program Development of Jiangsu Higher Education Institutions.

References

- Cao Y, Li P and Zhang Y (2018) Parallel processing algorithm for railway signal fault diagnosis data based on cloud computing. *Future Generation Computer Systems* 88: 279–283.
- Chen B, Shen B, Chen F, et al. (2019) Fault diagnosis method based on integration of rrsd and wavelet transform to rolling bearing. *Measurement* 131: 400–411.
- Chen J, Li K, Rong H, et al. (2018) A disease diagnosis and treatment recommendation system based on big data mining and cloud computing. *Information Sciences* 435: 124–149.
- Cheng J, Yang Y, Hu N, et al. (2021) A noise reduction method based on adaptive weighted symplectic geometry decomposition and its application in early gear fault diagnosis. *Mechanical Systems and Signal Processing* 149: 107351.
- Fan J, Qi Y, Gao X, et al. (2021) Compound fault diagnosis of rolling element bearings using multipoint sparsity–multipoint optimal minimum entropy deconvolution adjustment and adaptive resonance-based signal sparse decomposition. *Journal of Vibration and Control* 27: 1212–1230.
- Gai J, Shen J, Hu Y, et al. (2020) An integrated method based on hybrid grey wolf optimizer improved variational mode decomposition and deep neural network for fault diagnosis of rolling bearing. *Measurement* 162: 107901.
- Gong T, Yuan X, Yuan Y, et al. (2019) Application of tentative variational mode decomposition in fault feature detection of rolling element bearing. *Measurement* 135: 481–492.
- Hu J, Duan J, Chen Z, et al. (2018) Detecting impact signal in mechanical fault diagnosis under chaotic and gaussian background noise. *Mechanical Systems and Signal Processing* 99: 702–710.
- Huang W, Gao G, Li N, et al. (2018) Time-frequency squeezing and generalized demodulation combined for variable speed bearing fault diagnosis. *IEEE Transactions on Instrumentation and Measurement* 68: 2819–2829.
- Jia P, Yang J, Wu C, et al. (2019) Amplification of the lfm signal by using piecewise vibrational methods. *Journal of Vibration and Control* 25: 141–150.
- Leng Y, Wang T, Qin X, et al. (2004) Power spectrum research of twice sampling stochastic resonance response in a bistable system. *Acta Physica Sinica* 53: 717–723.
- Li F, Li R, Tian L, et al. (2019a) Data-driven time-frequency analysis method based on variational mode decomposition and its application to gear fault diagnosis in variable working conditions. *Mechanical Systems and Signal Processing* 116: 462–479.
- Li J, Zhang J, Li M, et al. (2019b) A novel adaptive stochastic resonance method based on coupled bistable systems and its application in rolling bearing fault diagnosis. *Mechanical Systems and Signal Processing* 114: 128–145.
- Li N, Huang W, Guo W, et al. (2019c) Multiple enhanced sparse decomposition for gearbox compound fault diagnosis. *IEEE Transactions on Instrumentation and Measurement* 69: 770–781.
- Li Y, Ding K, He G, et al. (2018) Non-stationary vibration feature extraction method based on sparse decomposition and order tracking for gearbox fault diagnosis. *Measurement* 124: 453–469.
- Li Y, Feng K, Liang X, et al. (2019d) A fault diagnosis method for planetary gearboxes under non-stationary working conditions using improved vold-kalman filter and multi-scale sample entropy. *Journal of Sound and Vibration* 439: 271–286.
- Liang P, Deng C, Wu J, et al. (2020) Intelligent fault diagnosis of rotating machinery via wavelet transform, generative adversarial nets and convolutional neural network. *Measurement* 159: 107768.
- Lonare S, Fernandes N and Abhyankar A (2021) Rolling element bearing multi-fault diagnosis using morphological joint time–frequency adaptive kernel–based semi-smart framework. *Journal of Vibration and Control*. DOI: [10.1177/10775463211022878](https://doi.org/10.1177/10775463211022878).
- Lu S, He Q, Hu F, et al. (2014) Sequential multiscale noise tuning stochastic resonance for train bearing fault diagnosis in an embedded system. *IEEE Transactions on Instrumentation and Measurement* 63: 106–116.
- Lu S, He Q and Wang J (2019) A review of stochastic resonance in rotating machine fault detection. *Mechanical Systems and Signal Processing* 116: 230–260.

- Lu S, He Q and Zhao J (2018) Bearing fault diagnosis of a permanent magnet synchronous motor via a fast and online order analysis method in an embedded system. *Mechanical Systems and Signal Processing* 113: 36–49.
- Lu S and Wang X (2018) A new methodology to estimate the rotating phase of a bldc motor with its application in variable-speed bearing fault diagnosis. *IEEE Transactions on Power Electronics* 33: 3399–3410.
- Qiao Z, Lei Y and Li N (2019) Applications of stochastic resonance to machinery fault detection: A review and tutorial. *Mechanical Systems and Signal Processing* 122: 502–536.
- Qin Y, Mao Y, Tang B, et al. (2019) M-band flexible wavelet transform and its application to the fault diagnosis of planetary gear transmission systems. *Mechanical Systems and Signal Processing* 134: 106298.
- Wang L, Cai G, Wang J, et al. (2019a) Dual-enhanced sparse decomposition for wind turbine gearbox fault diagnosis. *IEEE Transactions on Instrumentation and Measurement* 68: 450–461.
- Wang T and Leng Y (2003) Numerical research of twice sampling stochastic resonance for the detection of a weak signal submerged in a heavy noise. *Acta Physica Sinica* 52: 2432–2437.
- Wang Y, Tse PW, Tang B, et al. (2019b) Order spectrogram visualization for rolling bearing fault detection under speed variation conditions. *Mechanical Systems and Signal Processing* 122: 580–596.
- Yang J, Huang D, Zhou D, et al. (2020a) Optimal imf selection and unknown fault feature extraction for rolling bearings with different defect modes. *Measurement* 157: 107660.
- Yang J, Zhang S, Sanjuán MaF, et al. (2020b) Time-frequency analysis of a new aperiodic resonance. *Communications in Nonlinear Science and Numerical Simulation* 85: 105258.
- Yang T, Guo Y, Wu X, et al. (2018) Fault feature extraction based on combination of envelope order tracking and cica for rolling element bearings. *Mechanical Systems and Signal Processing* 113: 131–144.
- Yu G (2019) A concentrated time-frequency analysis tool for bearing fault diagnosis. *IEEE Transactions on Instrumentation and Measurement* 69: 371–381.
- Zhang H, Xiong W, Zhang S, et al. (2016) Nonstationary weak signal detection based on normalization stochastic resonance with varying parameters. *Sādhanā* 41: 621–632.
- Zhang J, Hou G, Ma B, et al. (2018a) Operating characteristic information extraction of flood discharge structure based on complete ensemble empirical mode decomposition with adaptive noise and permutation entropy. *Journal of Vibration and Control* 24: 5291–5301.
- Zhang J, Wu J, Hu B, et al. (2020a) Intelligent fault diagnosis of rolling bearings using variational mode decomposition and self-organizing feature map. *Journal of Vibration and Control* 26: 1886–1897.
- Zhang X, Liu Z, Miao Q, et al. (2018b) An optimized time varying filtering based empirical mode decomposition method with grey wolf optimizer for machinery fault diagnosis. *Journal of Sound and Vibration* 418: 55–78.
- Zhang Y, Ji J and Ma B (2020b) Fault diagnosis of reciprocating compressor using a novel ensemble empirical mode decomposition-convolutional deep belief network. *Measurement* 156: 107619.